Dynamic study of fusion reactions for ^{40,48}Ca+ ^{90,96}Zr around the Coulomb barrier

Ning Wang,[1,*] Xizhen Wu,[1,2,†] and Zhuxia Li[1,2,3,†]
[1]*China Institute of Atomic Energy, P. O. Box 275(18), Beijing 102413, People's Republic of China*
[2]*Nuclear Theory Center of National Laboratory of Heavy Ion Accelerator, Lanzhou 730000, People's Republic of China*
[3]*Institute of Theoretical Physics, Chinese Academy of Sciences, Beijing 100080, People's Republic of China*
(Received 24 September 2002; published 10 February 2003)

By using the updated improved quantum molecular dynamics model in which a surface-symmetry potential term has been introduced, the excitation functions for fusion reactions of ^{40,48}Ca+ ^{90,96}Zr at energies around the Coulomb barrier have been studied. The experimental data of the fusion cross sections for ^{40}Ca+ ^{90,96}Zr have been reproduced remarkably well without introducing any new parameters. The fusion cross sections for the neutron-rich fusion reactions of ^{48}Ca+ ^{90,96}Zr around the Coulomb barrier are predicted to be enhanced compared with a non-neutron-rich fusion reaction. In order to clarify the mechanism of the enhancement of the fusion cross sections for neutron-rich nuclear fusions, we pay great attention to studying the dynamic lowering of the Coulomb barrier during a neck formation. The isospin effect on the barrier lowering is investigated. It is interesting that the effect of the projectile and target nuclear structure on fusion dynamics can be revealed to a certain extent in our approach. The time evolution of the N/Z ratio at the neck region has been firstly illustrated. A large enhancement of the N/Z ratio at neck region for neutron-rich nuclear fusion reactions is found.

DOI: 10.1103/PhysRevC.67.024604 PACS number(s): 25.70.−z, 24.10.−i

I. INTRODUCTION

Being encouraged by the synthesis of superheavy elements, the investigation of the fusion mechanism at low energies has recently received a great deal of attention both theoretically and experimentally [1–8]. Since the central region of superheavy elements was predicted to be located at $Z=114$ or 120 and $N=184$, which is strongly neutron-rich, the study of the dynamics for neutron-rich fusion reactions is highly demanded for the purpose of the synthesis of superheavy elements. The dynamics of the fusion process for normal nuclear systems was studied in [9–15]. In these studies, it was shown that neck formation, dynamical deformation, etc., result in a lowering of the fusion barrier, and furthermore it was demonstrated that this lowering effect is mostly significant at energies near the barrier; consequently the subbarrier fusion cross sections are enhanced compared with the prediction of the WKB approximation. But for neutron-rich systems, the dynamics of the fusion process is much less studied. For neutron-rich systems, the symmetry term of EOS should play a significant dynamical role. Therefore, it seems to us that it is highly requisite to study how the symmetry potential influences the mechanism of neutron-rich fusion reaction process dynamically. In this work, we devote ourselves to study the fusion dynamics for neutron-rich systems at energies around the barrier by means of the improved quantum molecular dynamics (ImQMD) model [16]. In Ref. [16] we showed that the ImQMD model can describe the properties of the ground state of selected nuclei from ^{6}Li to ^{208}Pb very well with one set of parameters, and the experimental data of fusion reaction cross sections for ^{40}Ca + ^{90,96}Zr [7] can also be reproduced well with no extra parameters. From that study, the experimentally observed enhancement of fusion cross sections for ^{40}Ca+ ^{96}Zr compared with the non-neutron-rich fusion reaction of ^{40}Ca+ ^{90}Zr was attributed to a stronger dynamical lowering effect of the Coulomb barrier for the neutron-rich target reaction of ^{40}Ca+ ^{96}Zr. Based on that investigation, it would be very interesting to study the dynamics of fusion reactions induced by the neutron-rich projectile ^{48}Ca at energies around the Coulomb barrier with the same model. As is well known, ^{48}Ca has a double closed shell structure and a spherical shape the same as ^{40}Ca. Therefore, the static deformation effect of the projectile on the enhancement of fusion cross sections at energies around the barrier can be ruled out, and the role of the isospin effect should be shown by a comparison between the two cases. But, on the other hand, the shell structure of ^{48}Ca is rather different from ^{40}Ca, and the energy of the octupole vibrations of ^{48}Ca is about 1 MeV higher than that of ^{40}Ca due to the shell structure. Furthermore, from the inelastic scattering study it was shown that ^{40}Ca has a stronger octupole vibration than ^{48}Ca [6]. The situation is different for Zr isotopes for which the energy of the 3^- state decreases as the number of neutrons increases from ^{90}Zr to ^{96}Zr. This structure effect should influence the fusion dynamics and the fusion cross sections as well. It is not clear how to explicitly implement this effect into our model at this moment. However, a dynamical study of neutron-rich fusion reactions can provide us with information about dynamical deformation which may relate to the structure of the projectile and target, in addition to information about the isospin effect on a fusion process, which is quite general. In this work, we make a comparison of the dynamic barrier lowering effect for four reaction systems, ^{40,48}Ca+ ^{90,96}Zr, at energies around the barrier, and furthermore we analyze the causes for the dynamic barrier lowering in detail, mainly has focused on the stage of the neck formation and neck development.

*Email address: wangning@iris.ciae.ac.cn
†Email address: lizwux@iris.ciae.ac.cn

The paper is organized as follows. In Sec. II we briefly introduce our ImQMD model. Then we study the mechanism of neutron-rich nuclear fusion reactions in Sec. III. Finally, a short summary and discussion are given in Sec IV.

II. IMPROVED QMD MODEL

For reader convenience, in this section we briefly introduce the ImQMD model. In the ImQMD model, the same as in the original QMD model [17–20], each nucleon is represented by a coherent state of a Gaussian wave packet

$$\phi_i(\mathbf{r}) = \frac{1}{(2\pi\sigma_r^2)^{3/4}} \exp\left[-\frac{(\mathbf{r}-\mathbf{r}_i)^2}{4\sigma_r^2} + \frac{i}{\hbar}\mathbf{r}\cdot\mathbf{p}_i \right], \tag{1}$$

where $\mathbf{r}_i$ and $\mathbf{p}_i$ are the centers of the ith wave packet in the coordinate and momentum space, respectively. σ_r represents the spatial spread of the wave packet. Through a Wigner transformation of the wave function, the one-body phase space distribution function for N-distinguishable particles is given by

$$f(\mathbf{r},\mathbf{p}) = \sum_i f_i(\mathbf{r},\mathbf{p}), \tag{2}$$

where

$$f_i(\mathbf{r},\mathbf{p}) = \frac{1}{(\pi\hbar)^3} \exp\left[-\frac{(\mathbf{r}-\mathbf{r}_i)^2}{2\sigma_r^2} - \frac{2\sigma_r^2}{\hbar^2}(\mathbf{p}-\mathbf{p}_i)^2 \right]. \tag{3}$$

For identical fermions, the effects of the Pauli principle were discussed in a broader context by Feldmeier and Schnack [21]. The approximate treatment of antisymmetrization used in this paper is explained below. The density and momentum distribution function of a system read

$$\rho(\mathbf{r}) = \int f(\mathbf{r},\mathbf{p}) d^3p = \sum_i \rho_i(\mathbf{r}), \tag{4}$$

$$g(\mathbf{p}) = \int f(\mathbf{r},\mathbf{p}) d^3r = \sum_i g_i(\mathbf{p}), \tag{5}$$

respectively, where the sum runs over all particles in the system. $\rho_i(\mathbf{r})$ and $g_i(\mathbf{p})$ are the density and momentum distribution functions of nucleon i:

$$\rho_i(\mathbf{r}) = \frac{1}{(2\pi\sigma_r^2)^{3/2}} \exp\left[-\frac{(\mathbf{r}-\mathbf{r}_i)^2}{2\sigma_r^2} \right], \tag{6}$$

$$g_i(\mathbf{p}) = \frac{1}{(2\pi\sigma_p^2)^{3/2}} \exp\left[-\frac{(\mathbf{p}-\mathbf{p}_i)^2}{2\sigma_p^2} \right], \tag{7}$$

where σ_r and σ_p are the widths of wave packets in coordinate and momentum space, respectively, and they satisfy the minimum uncertainty relation [22]. The time evolution of $\mathbf{r}_i$ and $\mathbf{p}_i$ is governed by Hamiltonian equations of motion:

$$\dot{\mathbf{r}}_i = \frac{\partial H}{\partial \mathbf{p}_i}, \quad \dot{\mathbf{p}}_i = -\frac{\partial H}{\partial \mathbf{r}_i}. \tag{8}$$

The Hamiltonian H consists of the kinetic energy and the effective interaction potential energy:

$$H = T + U. \tag{9}$$

The effective interaction potential energy includes the nuclear local interaction potential energy and the Coulomb interaction potential energy:

$$U = U_{loc} + U_{coul}, \tag{10}$$

and

$$U_{loc} = \int V_{loc} d^3\mathbf{r}. \tag{11}$$

V_{loc} is the potential energy density, which can be derived directly from a zero-range Skyrme interaction [23,24]. Thus

$$U_{loc} = \frac{\alpha}{2}\sum_i \left\langle \frac{\rho}{\rho_0} \right\rangle_i + \frac{\beta}{3}\sum_i \left\langle \frac{\rho}{\rho_0} \right\rangle_i^2 + \frac{C_s}{2}\int \frac{(\rho_p-\rho_n)^2}{\rho_0} d^3\mathbf{r} + \int \frac{g_1}{2}(\nabla\rho)^2 d^3\mathbf{r}, \tag{12}$$

where

$$\langle\rho\rangle_i = \sum_{j\neq i} \rho_{ij} \tag{13}$$

and

$$\rho_{ij} = \frac{1}{(4\pi\sigma_r^2)^{3/2}} \exp\left[-\frac{(\mathbf{r}_i-\mathbf{r}_j)^2}{4\sigma_r^2} \right]. \tag{14}$$

The third term in the right hand side of Eq. (12) is the symmetry potential energy. The gradient term in U_{loc} accounts for the surface energy and the correction to the second term in Eq. (12) [16,23].

Because in this work we are going to study the isospin effect on the fusion dynamics in neutron-rich nuclear fusion reactions, we pay special attention to the symmetry potential term. Therefore, we make a more careful treatment on the symmetry potential term; that is, in addition to the volume symmetry potential term, we further introduce a surface symmetry potential term according to the finite-range liquid-drop model [25], which reads

$$U_{sur-sym} = \frac{C_s C_k}{2\rho_0} \sum_{i,j\neq i} s_i s_j \rho_{ij} \nabla_i^2 \rho_{ij}, \tag{15}$$

where, s_i is $+1$ for a proton and -1 for a neutron, and C_k is the strength parameter for the surface symmetry term. We find that this term plays an important dynamical role for reactions ^{48}Ca+ ^{90,96}Zr, but a minor role for ^{40}Ca+ ^{90,96}Zr. It reduces the fusion cross sections for ^{48}Ca+ ^{90,96}Zr considerably, but almost does not change the cross sections of

TABLE I. The parameters used in the calculations.

α(GeV)	β(GeV)	ρ_0(fm^{-3})	g_0(GeV fm^5)	C_s(GeV)	C_k(fm^5)
−0.124	0.071	0.165	0.96	0.032	1.0

^{40}Ca+ ^{90,96}Zr. A discussion of the effect of this term will be given elsewhere. The parameters used in this work are listed in Table I.

Considering the fact that for a finite system the nucleons are localized in a finite region corresponding to the size of the system, the width of the wave packets representing nucleons in the system should have a relation to the size of the system. As in Ref. [16], here we also adopt a system size dependent wave packet width to account for the fact, that is,

$$\sigma_r = 0.16N^{1/3} + 0.49, \tag{16}$$

where N is the number of nucleons bound in the system.

In order to overcome the difficulty in describing the Fermionic nature of an N-body system in the QMD model, an approximate treatment of antisymmetrization is adopted, namely, we implement the phase space constraint of the CoMD model proposed by Papa *et al.* [26] into the model. This is required by the constraint that the one body occupation number in a volume h^3 of phase space centered at $(\mathbf{r_i},\mathbf{p_i})$, corresponding to the centroid of the wave packet of particle i, should always be not larger than 1 according to the Pauli principle. The one body occupation number is calculated by

$$f_i^{ocu} = \sum_j \delta_{\tau_i\tau_j}\delta_{s_i,s_j}\int_{h^3} f_j(\mathbf{r},\mathbf{p})d^3\mathbf{r}d^3\mathbf{p}, \tag{17}$$

where s_i and τ_i are the third components of the spin and isospin of particle i. We have made a check of the time evolution of individual nuclei from light nuclei to heavy nuclei, and found that by using the procedure of phase space constraint, the requirement is reasonably satisfied and the phase space distribution is efficiently prevented from evolving into a classical distribution from the initial nuclear ground state distribution for a long enough time.

Concerning the collision part, an isospin dependent nucleon-nucleon scattering cross section and Pauli blocking are used [27,11]. This part actually plays a minor role in a fusion reaction.

In this work the initial density distribution of the projectile and target is obtained by Skyrme Hartree-Fock calculations [28–30]. The other procedures are the same as in Ref. [16]. The model was carefully checked, and it turns out that the ImQMD model works well in describing the ground state properties for nuclei from ^{6}Li to ^{208}Pb, and calculating the static Coulomb barrier for fusion reactions as well as fusion cross sections for ^{40}Ca+ ^{90,96}Zr.

III. RESULTS

Before coming to the numerical results for fusion reactions ^{40,48}Ca+ ^{90,96}Zr, let us first make a survey of the configurations along a fusion path. In Fig. 1 we illustrate one typical fusion event of the head on reaction of ^{40}Ca+ ^{90}Zr at an energy 5 MeV below the barrier. In the figure, we plot the dynamical barrier V_b as a function of the distance between the center of mass of projectile and that of the target. We will discuss the dynamical barrier in more detail in the following section (Sec. III B) and the definition of it will be given there. Simultaneously, in subfigures we plot the contour plots of density distributions as well as the corresponding single-particle potentials at three typical times, i.e., before, at, and after reaching the highest value of the dynamic barrier along the fusion path. The single-particle potential is calculated by

$$V_{sp}(\mathbf{r}) = \int \rho(\mathbf{r}')V(\mathbf{r}-\mathbf{r}')d^3\mathbf{r}', \tag{18}$$

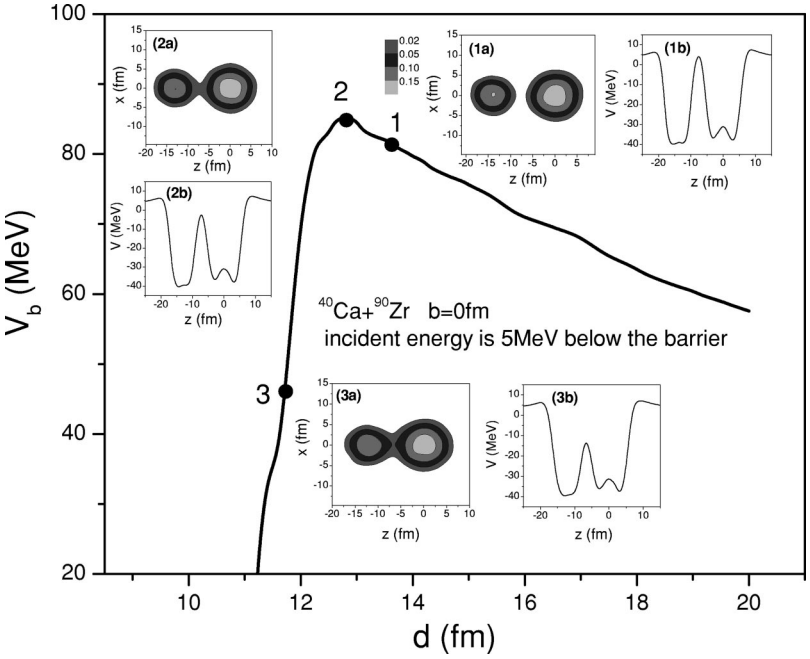

FIG. 1. The fusion path for a typical event of a head on reaction of ^{40}Ca+ ^{90}Zr at the energy 5 MeV below the Coulomb barrier. The thick curve is the dynamical barrier as a function of the distance between the centers of mass of projectile and target. Subfigures (1a), (2a), and (3a) are for contour plots of the density distributions of the reaction systems at the corresponding time pointed in the curve of $V_b \sim d$, and (1b), (2b), and (3b) are the corresponding single-particle potentials at the same time as subfigures (1a), (2a), and (3a).

with $\rho(\mathbf{r})$ being the density distribution of the system and $V(\mathbf{r}-\mathbf{r}')$ the effective nucleon-nucleon interaction. In subfigures (1a) and (1b) we plot the contour plot of the density distribution as well as the corresponding single-particle potential at point 1 along the fusion path. One can find from these two subfigures that at this point the fusion partners are not in touch [see subfigure (1a)], and there is a high enough inner potential barrier which prevents nucleons from moving from the projectile to the target, or vice versa [see subfigure (1b)]. At the time, corresponding to point 2, the dynamic barrier reaches a maximum value. The contour plot of the density distribution [subfigure (2a)] shows that the fusion partners are at a touching configuration, and that a neck starts to grow and, following this, the inner potential barrier in the potential well is reduced, allowing a few nucleons to move from a projectile to a target, or vice versa [see subfigure (2b)]. At a time corresponding to point 3, the dynamical barrier is reduced considerably. Subfigures (3a) and (3b) show that the neck develops considerably at this time and, consequently, the inner potential barrier in the potential well is reduced substantially, and nucleon transfer between the projectile and target becomes much easier than before. This means that a precompound nucleus begins to be formed. From this study we have learned how the dynamical fusion barrier is correlated with the development of the configuration of fusion partners along the fusion path.

In the following, we show the numerical results for fusion reactions ^{40,48}Ca+ ^{90,96}Zr. First we show the fusion cross sections. For understanding the mechanism of the enhancement of the fusion cross sections for ^{40}Ca+ ^{96}Zr and ^{48}Ca + ^{90,96}Zr compared with the ^{40}Ca+ ^{90}Zr case, we show the dynamic barrier and other quantities relevant to the dynamic lowering of the Coulomb barrier only at head on reactions. Following this we discuss the isospin and structure effect in fusion dynamics for the systems studied. In order to explore how the isospin is transferred at the neck region, we study the time evolution of the N/Z ratio at the neck region for ^{40,48}Ca+ ^{90,96}Zr reactions to see how it depends on the initial N/Z ratio.

A. Fusion cross sections for ^{40,48}Ca+ ^{90,96}Zr

After making the preparation of the initial nuclei, we elaborately select ten projectile nuclei and ten target nuclei from thousands of preprepared systems. By rotating these prepared projectile and target nuclei around their centers of mass by a Euler angle chosen randomly, we create 100 bombarding events for each reaction energy E and impact parameter b. By counting the number of fusion events, we obtain the probability of fusion reaction $g_{fus}(E,b)$, then the cross section is calculated by using the expression

$$\sigma_{fus}=2\pi\int_0^{b_{\max}} b g_{fus}(E,b)db=2\pi\sum\ b g_{fus}(E,b)\Delta b. \tag{19}$$

The distance from the projectile to the target at an initial time is taken to be 20 fm.

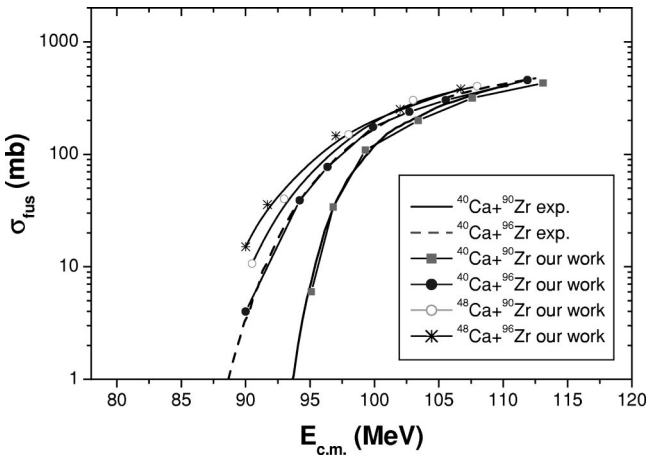

FIG. 2. The fusion cross sections for ^{40,48}Ca+ ^{90,96}Zr. The experimental data are taken from [7].

For the definition of the fusion event, we adopt the same operational definition as in TDHF calculations and in the QMD model calculations [31]. More specifically, in this work we consider any event, for which the number of nucleons escaping during the process form compound nuclei is equal to or less than 6, as a fusion event [16]. Figure 2 shows the fusion cross sections for ^{40}Ca+ ^{90}Zr, ^{40}Ca+ ^{96}Zr, ^{40}Ca + ^{90}Zr, and ^{40}Ca+ ^{90}Zr, respectively. Experimental data for the reactions of ^{40}Ca+ ^{90,96}Zr, taken from Ref. [7], are also shown. One can see that the experimental data for ^{40}Ca + ^{90,96}Zr are reproduced well without introducing new parameters, and that there is a strong enhancement of the fusion cross sections for neutron-rich reactions. The fusion cross sections for reactions ^{48}Ca+ ^{90,96}Zr at energies around the barrier are higher than those for ^{40}Ca+ ^{96}Zr. But the enhancement of the fusion cross sections for ^{48}Ca+ ^{90,96}Zr compared with ^{40}Ca+ ^{96}Zr is not so strong as the case of ^{40}Ca+ ^{96}Zr compared with ^{40}Ca+ ^{90}Zr. For understanding the feature of the fusion excitation functions for different systems shown in Fig. 2, let us first look at the distribution of fusion probabilities with respect to the impact parameters in Fig. 3. In the figure one finds that, for neutron-rich reactions, in addition to having a larger fusion probability, the maximum impact parameter leading to fusion is larger compared with non-neutron-rich reactions. For example, at an incident energy of 5 MeV below the static Coulomb barrier, the maximum impact parameter leading to fusion is about 9 fm for reaction ^{48}Ca+ ^{90,96}Zr, about 8.5 fm for ^{40}Ca+ ^{96}Zr, and only 6.5 fm for the non-neutron-rich reaction of ^{40}Ca + ^{90}Zr. This means that, for neutron-rich reactions, the fusion partners can be fused at a relative the larger distance. A possible reason for this is that the dynamical elongation is enhanced for neutron-rich fusion systems. The effect of the dynamical elongation on the dynamical lowering of the Coulomb barrier will be discussed in Sec. III B.

For the cases of the incident energy at 10 MeV above the static Coulomb barrier, the distribution of the fusion probability with respect to the impact parameter shows a similar tendency, but the effect is weaker.

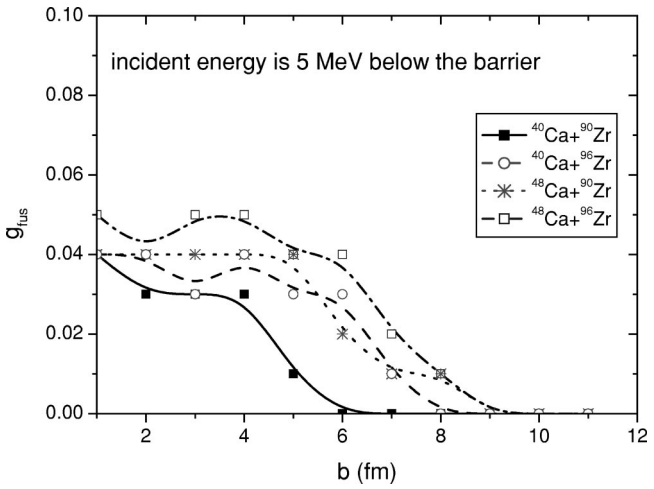

FIG. 3. The distributions of the fusion probability for reactions of ^{40,48}Ca+ ^{90,96}Zr with respect to impact parameters.

B. Dynamic lowering of the barrier

In order to understand the reason for the enhancement of fusion reaction cross sections for neutron-rich nuclear fusions, in this section we study the dynamic Coulomb barrier lowering effect. In the QMD model, the Coulomb barrier is calculated microscopically by using the expressions

$$V_b(d)=\int d^3r_1 \int d^3r_2 \rho_1(\mathbf{r}_1-\mathbf{r}_{1c})V(\mathbf{r}_1-\mathbf{r}_2)\rho_2(\mathbf{r}_2-\mathbf{r}_{2c}), \tag{20}$$

$$d=|\mathbf{r}_{1c}-\mathbf{r}_{2c}|,$$

where ρ_1 and ρ_2 are the density distribution of the projectile and target, respectively; $\mathbf{r}_{1c}$ and $\mathbf{r}_{2c}$ are their centers of mass, respectively. $V(\mathbf{r}-\mathbf{r}')$ is the effective nucleon-nucleon interaction. It is clear that, in general, $V_b(d)$ is a function of time since ρ_1 and ρ_2 change from time to time. Only in a static case, the density distribution of the projectile and target is assumed to be the same as that at the initial time; correspondingly the static barrier is calculated with the static density distribution. Therefore, for the static barrier, the dynamical effects experienced by fusion partners during a reaction process are not taken into account. For the dynamic case, the density distributions of the projectile and target are calculated by using expression (4) with the sum running over all particles in the projectile and target, respectively. When two colliding partners approach each other, the density distributions of the projectile and target change from time to time and their shapes (determined by the density distribution) are deformed due to the interaction between them. The time evolution of the shape deformation and the neck formation depends on the incident system and energy as well as the impact parameter. Consequently, the dynamical barrier not only depends on the incident system but also depends on the incident energy as well as the impact parameter. In the following we only study the head on collision case, and define the height of the highest Coulomb barrier experienced in the path of fusion as the height of the dynamic Coulomb barrier.

Generally, the dynamic barrier is lower than the static barrier because of the neck formation and the increase of the N/Z ratio at the neck region for neutron-rich nuclear fusion reactions. As an example, in Table II we show the results for the dynamic barrier for head on fusion reactions of ^{40,48}Ca + ^{90,96}Zr at energies 5 MeV below and 10 MeV above the static Coulomb barrier. From this table one can see that the dynamic effect lowers the height of the barrier dramatically, and this dynamic lowering is incident energy and system dependent. The barrier lowering is stronger for the case of the energy below the barrier than that of the energy above the barrier. This feature of barrier lowering was also observed in Ref. [15] for symmetric reactions of oxygen and nickel isotopes by means of the mean field transport theory.

To illustrate the system dependence of the dynamic barrier, in Fig. 4 we show the time evolution of the dynamic barrier for head on collisions of ^{40,48}Ca+ ^{90,96}Zr at an incident energy 5 MeV below the static barrier. From a comparison among four curves we see the following trends: (1) The dynamic Coulomb barrier for neutron-rich reactions is lower than that for non-neutron-rich reactions. (2) The barrier top position for neutron-rich reactions is shifted to a larger distance compared to non-neutron-rich ones. (3) The width of the barrier for neutron-rich reactions is thinner than that for non-neutron-rich reactions. As for three neutron-rich reactions, there is no obvious difference in the dynamic Coulomb barrier.

To investigate the causes leading to these trends, let us turn to study the quantities relevant to the dynamic barrier. For the purpose of understanding the mechanism, in Table III we give only the calculation results for head on collisions of ^{40,48}Ca+ ^{90,96}Zr at energies of 5 MeV below (lower energy

TABLE II. The comparison between the static Coulomb barrier and the dynamic barrier for reactions of ^{40,48}Ca+ ^{90,96}Zr.

Reaction	^{40}Ca+ ^{90}Zr		^{40}Ca+ ^{96}Zr		^{48}Ca+ ^{90}Zr		^{48}Ca+ ^{96}Zr	
$E_{\text{c.m.}}$(MeV)	93.8	108.8	92.3	107.3	92.5	107.5	92.1	107.1
Time reaching the top of barrier (fm/c)	171	141	172	142	176	146	177	145
Height of dynamic barrier (MeV)	85.7	88.6	83.8	87.5	84.3	87.2	84.0	86.5
Dynamic lowering (MeV)	13.1	10.2	13.5	9.8	13.2	10.3	13.1	10.6
Height of static barrier (MeV)	98.8		97.3		97.5		97.1	

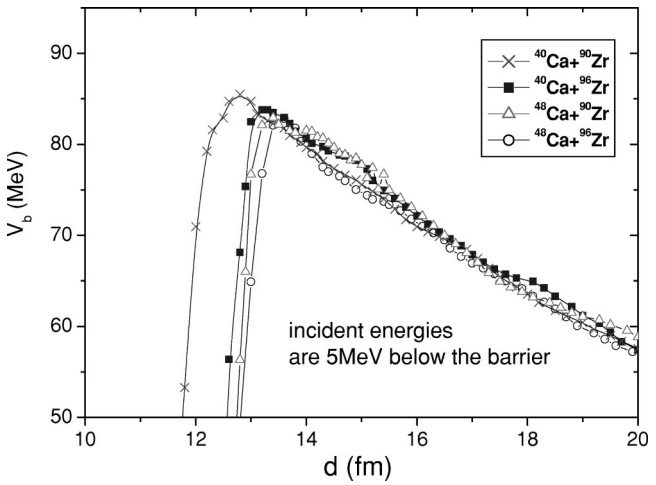

FIG. 4. The dynamic barriers as a function of the distance of the center of mass projectile and the target for head on collisions of ^{40,48}Ca+ ^{90,96}Zr at the incident energy of 5 MeV below the static Coulomb barrier.

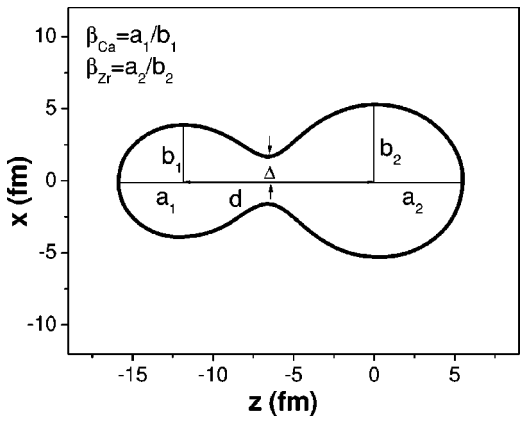

FIG. 5. The definition of the geometric quantities in Table III.

case) and 10 MeV above (higher energy case) the corresponding static Coulomb barrier. The quantities listed in Table III are calculated as follows: for each event, we calculate the $V_b(d)$ at each time step to find the time needed to reach the highest barrier (i.e., point 2 in Fig. 1). The contour map with $\rho=0.02/\mathrm{fm}^3$ of the density distribution of the system at this time gives the shape of the system [see subfigure (2a) of Fig. 1]. The schematic figure of Fig. 5 illustrates the shape of the system (typically for a head on collision) at this time, and the geometry quantities listed in Table III, such as the distance between the centers of mass of projectile and target, and the neck radius, etc., are shown in the figure. The results given in Table III are the average values of all corresponding events. The elongation given in Table III is equal to the distance between the centers of mass of the projectile and target minus the radii of the initial projectile and target nuclei. From Table III one can find that the height of the dynamic barrier is closely correlated with the elongations obtained for different incident energies and collision systems listed in the table, i.e., the larger the elongation the lower the barrier. Generally speaking, the elongation at the touching configuration should depend on the interaction time before reaching the touching configuration, and the longer interaction time leads to a larger elongation. Therefore, the elongation for the lower energy case is always larger than that for the higher energy case. Table III shows that the elongation for energy below the static barrier case is about 10 % larger than that for above the static barrier case. Furthermore, the elongation also depends on the structure of the projectile and target and the N/Z ratio at the neck region as well. Now let us look at the dependence of the elongation on the structure of reaction systems. For the lower energy case, the largest elongation is obtained in the reaction of ^{40}Ca+ ^{96}Zr, while for the higher energy case the largest elongation is obtained in ^{48}Ca+ ^{96}Zr. As is well known that the energy of octupole vibration of ^{96}Zr is lower than that of ^{90}Zr, and we may consider that ^{96}Zr is softer than ^{90}Zr. For ^{48}Ca, the energy of the octupole vibration is about 1 MeV higher than that of ^{40}Ca, which implies that ^{48}Ca is more rigid than ^{40}Ca. The dependence of the elongation on the different systems given in Table III clearly shows the influence of the nuclear structure effect. Concerning the isospin effect, it is quite natural that the increase of N/Z at the neck region should decrease

TABLE III. The quantities relevant to the dynamic barrier calculated at the time when the dynamic barrier reaches the highest value in the fusion path.

Reaction	^{40}Ca+ ^{90}Zr		^{40}Ca+ ^{96}Zr		^{48}Ca+ ^{90}Zr		^{48}Ca+ ^{96}Zr	
$E_{\mathrm{c.m.}}$(MeV)	93.8	108.8	92.3	107.3	92.5	107.5	92.1	107.1
Height of dynamic barrier (MeV)	85.7	88.6	83.8	87.5	84.3	87.2	84.0	86.5
Distance between centers of mass **d** (fm)	13.01	12.50	13.24	12.72	13.26	12.78	13.40	12.96
Elongation (fm)	5.23	4.72	5.35	4.83	5.31	4.83	5.34	4.90
N/Z at neck region	1.210	1.165	1.407	1.323	1.468	1.360	1.610	1.577
Width of neck Δ (fm)	1.92	2.22	1.89	2.15	1.91	2.20	1.95	2.16
ρ at neck (fm^{-3})	0.027	0.029	0.027	0.028	0.027	0.029	0.027	0.027
N/Z of total system	1.167		1.267		1.300		1.400	

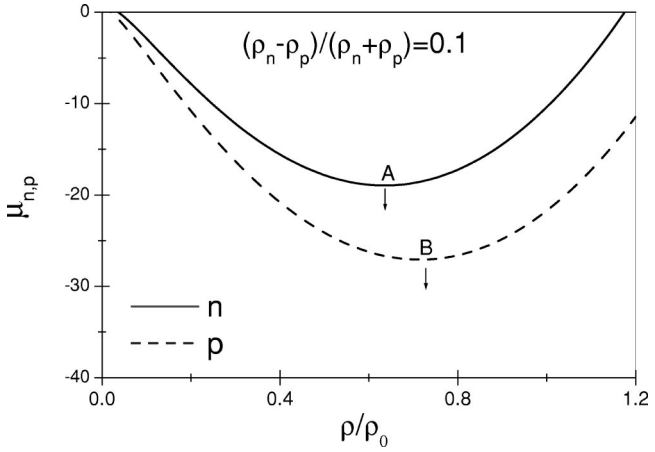

FIG. 6. The density dependence of the chemical potential of protons and neutrons for neutron rich systems.

the height of the Coulomb barrier. There is a strong enhancement of the N/Z ratio at neck region for neutron-rich reactions, as shown in Table III. Consequently, for ^{40}Ca+ ^{96}Zr compared with ^{40}Ca+ ^{90}Zr, both the isospin effect and the structure effect are in favor of enhancing the fusion cross sections of ^{40}Ca+ ^{96}Zr. While for reactions induced by the ^{48}Ca compared with reactions induced by ^{40}Ca, the isospin effect and the structure effect are counterparts; consequently the enhancement of the fusion cross section induced by the neutron-rich effect is reduced by the structure effect.

C. Time evolution of the *N/Z* ratio at the neck region

As seen from the above study, the dynamic lowering of the barrier is closely related to the configuration and component of the neck. The N/Z ratio at the neck region is one of the most sensitive quantities with respect to the neck formation for neutron-rich nuclear fusion reactions, as shown in Table III. For the isospin symmetry case of ^{40}Ca+ ^{90}Zr, the N/Z ratio at the neck region is more or less the same as the average N/Z ratio of the total system. But for the neutron-rich reactions, the N/Z ratio at the neck region is much higher than that of the average N/Z value of the corresponding systems. This effect results from the different behavior of the density dependence of the chemical potential for neutrons and protons in isospin asymmetry systems. The chemical potential is defined as

$$\mu_{n/p}=\frac{\partial\varepsilon(\rho,\delta)}{\partial\rho_{n/p}}, \tag{21}$$

where $\varepsilon(\rho,\delta)$ is the energy density and $\mu_{n/p}$ and $\rho_{n/p}$ are the chemical potential and the density of neutrons and protons, respectively. From the definition one can find that the chemical potential is a function of both the density ρ and the isospin asymmetry δ. Figure 6 shows the chemical potential of the proton and neutron as a function of density with $\delta=(N-Z)/(N+Z)=0.10$. From Fig. 6 one can see that the density corresponding to the minimum of the chemical potential of neutrons is lower than that of protons for a neutron-rich nuclear system, and thus the neutrons are preferably driven to the lower density area. This effect has also been studied, and confirmed in the intermediate energy heavy ion collisions. The increase of the N/Z ratio at the neck region should reduce the dynamic barrier in the fusion process. It would be interesting to study the isospin transfer at the neck region; therefore, in Fig. 7 we show the time evolution of the N/Z ratio at the neck region for head on fusion reactions of ^{40,48}Ca+ ^{90,96}Zr at energies 5 MeV below and 10 MeV above the static Coulomb barrier, in which the time starts from the beginning of the neck formation (when the density at the touching point reaches $0.02\rho_0$). The general trend of the time evolution of the N/Z ratio is the following: the N/Z ratio at the neck region first increases as time increases, then soon reaches a maximum value and then decreases, finally it approaches the average N/Z value of the system. The figure shows that the enhancement of N/Z at the neck region at the early stage of the neck formation strongly depends on the N/Z ratio of the initial system, i.e., the larger the isospin asymmetry of the initial system is, the stronger the enhancement of N/Z ratio at neck region. The reason for the fluctuation appearing in the time evolution of the N/Z ratio for neutron-rich reactions may be understood as follows: at the beginning when the neck is just formed, neutrons preferably move to the neck region driven by the chemical potential; not soon, as too many neutrons are concentrated there, the symmetry potential attracts more protons to migrate into the neck region and the N/Z ratio is reduced; then, because of the increase of the proton number the Coulomb repulsion plays a role. Thus the interplay of the Coulomb force and the symmetry potential results in a fluctuation behavior in the time evolution of the N/Z ratio at the neck region for

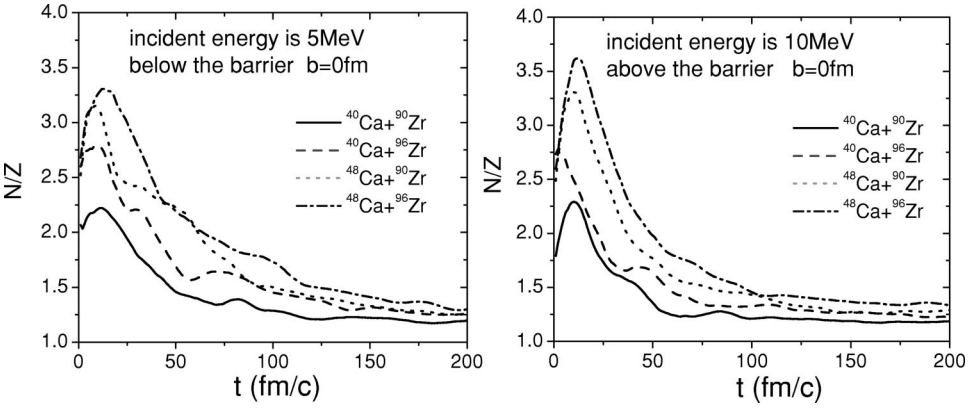

FIG. 7. The time evolution of the N/Z ratio at the neck region for fusion reactions of ^{40,48}Ca + ^{90,96}Zr. The right panel is for the case at the energy of 10 MeV above the static Coulomb barrier, and the left panel is for the case at the energy of 5 MeV below the static Coulomb barrier.

neutron-rich systems. This fluctuation becomes stronger for noncentral collisions. With the growth of the neck, nucleon transfer through the neck becomes easier and the fusion system passes over the dynamic barrier. After about 100 fm/c, that is, when a neck develops well, the N/Z ratio at the neck region gradually approaches the average N/Z ratio of the whole system, and the isospin degree of freedom seems to gradually reach an equilibrium; but the dissipation of the collective motion is still going on. The details of the nucleon transfer and the dissipation of the collective motion in the neck region will be discussed elsewhere.

IV. SUMMARY AND DISCUSSION

In this work we have introduced a surface-symmetry potential term into a QMD-type transport model. We have used this updated ImQMD model to study the fusion dynamics of ^{40,48}Ca+ ^{90,96}Zr at energies around the barrier. The surface-symmetry term seems to play an important role in fusion dynamics for ^{48}Ca+ ^{90,96}Zr, but a negligible role in that of ^{40}Ca+ ^{90,96}Zr. Our calculated results of excitation functions for fusion reactions of ^{40,48}Ca+ ^{90,96}Zr show a strong enhancement of fusion cross sections for the neutron-rich reactions at energies near and below the static barrier. We have made a systematic analysis to understand this feature. We have shown that the maximum impact parameter leading to a fusion reaction for neutron-rich reactions is larger than that for non-neutron-rich reactions, which means that the excess neutrons make the reaction partners to be fused at longer distance.

We have paid great attention to a study of the dynamical fusion barrier, and found that there is a substantial lowering of the dynamic barrier compared with the static Coulomb barrier due to the neck formation. For the reactions studied we have observed the following: (1) The dynamic Coulomb barrier for a neutron-rich configuration is lower than that for a non-neutron-rich case; (2) The barrier top position for a neutron-rich configuration is shifted to a larger distance compared to a non-neutron-rich configuration. (3) The width of the barrier for a neutron-rich configuration is thinner than that for a non-neutron-rich case.

We have shown that the time evolution of the ratio of neutrons to protons (the N/Z ratio) at the neck region strongly depends on the projectile and target isospin. At the early stage of the neck formation, the N/Z ratio at neck region can reach a value of twice the average N/Z ratio value of the whole system for ^{48}Ca+ ^{90,96}Zr; then, 100 fm/c later, the N/Z ratio at the neck region gradually approaches the average value of the whole system, which means that the isospin degree of freedom gradually approaches an equilibrium before the dissipation of the collective motion is completed.

A strong enhancement of fusion cross sections for ^{40}Ca + ^{96}Zr compared to ^{40}Ca+ ^{90}Zr have been found, which is in good agreement with the observation in experiments. Relatively, the enhancement of fusion cross sections for ^{48}Ca + ^{90,96}Zr compared with ^{40}Ca+ ^{96}Zr is less strong. The dynamic barrier lowering has been studied systematically. We find it relates strongly to the elongation of systems and the N/Z ratio at the neck region at the touching configuration on the fusion path. The results seem to show that the elongation at the touching configuration for different reaction systems is correlated with the structure of the projectile and target. For instance, the largest elongation is obtained in the case of ^{40}Ca+ ^{96}Zr at 5 MeV below the static barrier, consistent with the fact that the energy of the octupole vibration decreases from ^{90}Zr to ^{96}Zr and from ^{48}Ca to ^{40}Ca as well. On the other hand, the isospin effect which strongly influences the N/Z ratio at the neck region for neutron-rich nuclear fusion should affect the dynamic barrier strongly and, consequently, affect the fusion cross sections of neutron-rich nuclear reactions. Further work on exploring how the isospin effect and the structure effect compete in fusion reactions is needed. We strongly urge future measurements of the fusion cross section and the distribution of the barrier for ^{40,48}Ca+ ^{90,96}Zr to explore the interplay between these two effects in fusion reactions.

The problem concerning the mass transfer has not yet been discussed, and the neck dynamics is not discussed thoroughly in this paper. Work on these aspects is in progress.

ACKNOWLEDGMENTS

We thank Professor H. Q. Zhang and Professor Z. H. Liu for stimulating discussions. The work was supported by the National Natural Science Foundation of China under Grant Nos. 19975073, 10175093, and 10175089, and by the Science Foundation of Chinese Nuclear Industry and Major State Basic Research Development Program under Contract No. G20000774.

[1] V.I. Zagrebaev, Phys. Rev. C **64**, 034606 (2001).
[2] A. Diaz-Torres, G.G. Adamian, N.V. Antonenko, and W. Scheid, Phys. Lett. B **481**, 228 (2000).
[3] G.G. Adamian, N.V. Antonenko, A. Diaz-Torres, and W. Scheid, Nucl. Phys. **A671**, 233 (2000).
[4] Toshiki Maruyama, A. Bonasera, Massimo Papa, and S. Chiba, nucl-th/0107021.
[5] Y. Aritomo, T. Wada, M. Ohta, and Y. Abe, in *Proceedings on Fusion Dynamics at the Extremes, Dubna, 2000*, edited by Yu. Oganessian and V. Zagrebaev (World Scientific, Singapore, 2001), p. 123; Y. Abe, C.W. Shen, and G. Kosenko, in *Non-equilibrium and Nonlinear Dynamics in Nuclear and other Finite Systems, Beijing 2001*, edited by Z. Li, K. Wu, X. Wu, E. Zhao, and F. Sakata, AIP Conf. Proc. No. 597 (AIP, New York, 2001), p. 209.
[6] M. Trotta *et al.*, Phys. Rev. C **65**, 011601(R) (2001).
[7] H. Timmers, D. Ackermann, S. Beghini, L. Corradi, J.H. He, G. Montagnoli, F. Scarlassara, A.M. Stefanini, and N. Rowley, Nucl. Phys. **A633**, 421 (1998).
[8] Yu. Oganessian *et al.*, Phys. Rev. **63**, 011301(R) (2001).
[9] M. Beckerman, Phys. Rep. **129**, 145 (1985); Rep. Prog. Phys. **51**, 1047 (1988).

[10] R. Vandenbosch, Ann. Rev. Nucl. **44**, 447 (1992).
[11] W. Reisdorf, J. Phys. G **20**, 1297 (1994).
[12] A.B. Balantekin and N. Takigawa, Rev. Mod. Phys. **70**, 77 (1998).
[13] Proceedings of the International Workshop on ''Heavy Ion Collisions at Near Barrier Energies'' [J. Phys. G **23**, 1157 (1997)].
[14] K. Hagino, N. Takigawa, M. Dasgupta, D.J. Hinde, and J.R. Leigh, Phys. Rev. Lett. **79**, 2014 (1997); K. Hagino, N. Takigawa, and S. Kuyucak, *ibid.* **79**, 2943 (1997).
[15] V.N. Kondratyev, A. Bonasera, and A. Iwamoto, Phys. Rev. C **61**, 044613 (2000).
[16] Ning Wang, Zhuxia Li, and Xizhen Wu, Phys. Rev. C **65**, 064608 (2002).
[17] Ch. Hartnack, Zhuxia Li, L. Neise, G. Peilert, A. Rosenhauser, H. Sorge, J. Aichelin, H. Stoecker, and W. Greiner, Nucl. Phys. **A495**, 303 (1989); Zhuxia Li, Ch. Hartnack, H. Stoecker, and W. Greiner, Phys. Rev. C **40**, 824 (1991).
[18] J. Aichelin, Phys. Rep. **202**, 233 (1991), and references therein.
[19] Ch. Hartnack, Rajeev K. Puri, and J. Aichelin, Eur. Phys. J. A **1**, 151 (1998).
[20] A. Ono, H. Horiuchi, Toshiki Maruyama, and A. Ohnishi, Phys. Rev. Lett. **68**, 2898 (1992); Y. Kanada-En'yo and H. Horiuchi, Phys. Rev. C **52**, 647 (1995); Y. Kanada-En'yo, H. Horiuchi, and A. Doté, *ibid.* **60**, 064304 (1999).
[21] H. Feldmeier and J. Schnack, Rev. Mod. Phys. **72**, 655 (2000).
[22] H. Feldmeier and J. Schnack, Prog. Part. Nucl. Phys. **39**, 392 (1997), and references therein.
[23] David H. Boal and James N. Glosi, Phys. Rev. C **37**, 91 (1988); **38**, 2621 (1988).
[24] D. Vautherin and D.M. Brink, Phys. Rev. C **5**, 626 (1972).
[25] P. Möller, J.R. Nix, W.D. Myers, and W.J. Swiatescki, At. Data Nuclear Data Tables **59**, 185 (1995).
[26] Massimo Papa, Toshiki Maruyama, and Aldo Bonasera, Phys. Rev. C **64**, 024612 (2001).
[27] Qingfeng Li and Zhuxia Li, Phys. Rev. C **64**, 064612 (2001).
[28] I. Hamamoto, H. Sagawa, and X.Z. Zhang, Phys. Rev. C **53**, 765 (1996).
[29] I. Hamamoto, H. Sagawa, and X.Z. Zhang, Nucl. Phys. **648**, 203 (1999).
[30] M.A. Preston and R.K. Bhaduri, *Structure of the Nucleus* (Addison-Wesley, Reading, MA, 1975), pp. 10–14.
[31] T. Maruyama *et al.*, Phys. Rev. C **57**, 655 (1998).